Energy supply performance of air-, water-, and dual-cooled PV/T systems in different climatic zones of China

Peiyuan Xu[1,*] and Jinkun Zheng[2]

[1]University of Kassel, Mönchebergstr. 19, 34125, Kassel, Germany.
[2]Jinan Petrochemical Design Institute, Yishou Road 1, Lixia District, Jinan, China.

*799506217@qq.com

Abstract. This paper investigates the performance of PV/ T (photovoltaic/ thermal) system operating in air-cooling, water-cooling and dual-cooled scenarios in different climatic zones in China, and explores the effects of different coolant on the efficiency of PV/T systems, which can provide references for the design of PV/T systems in China. In this paper, the corresponding simple mechanism models are created in the Python. Since the devices to be simulated can be regarded as white-box, their reliability can be guaranteed. The operation of PV/T collectors with air-cooling, water-cooling and dual-cooled as heat dissipation systems in different regions is simulated by means of mathematical modeling, respectively, and the reliability of the mathematical model is verified by some previous studies. The results show that when the coolant flow rates are both 0.03 kg/s, the dual-cooling system, when considering the system power generation efficiency, gives a gain of 5.34 in the better performing region, an imperceptible advantage over the water-cooling system. However, without considering the fresh air supply, the water-cooling system has a clear advantage in terms of the total efficiency of solar energy utilization, which can reach 82.38% in the better-performing region, compared to the dual-cooled system, which has a slightly lower total efficiency of 76.52%. Therefore, in most cases, water-cooling system is the optimal solution to maximize the total efficiency. When only pursuing the efficiency of photovoltaic power generation, the dual cooling system only has a theoretical advantage over the water-cooling system, however, when taking into cost, this option is not recommended.

Keywords: Photovoltaic, Photothermal, dual-cooled, collector, PV/T.

1 Introduction

Replacing thermal power generation with clean energy generation is a necessary part of realizing environmental protection. In China, the Government has made many efforts to this end. However, the investment in research and development of PV in the early stage is insufficient, meanwhile, subsidies are not strong enough to make photovoltaics become more economically acceptable and replace thermal power [1]. The disecono

A. E. Abomohra et al. (eds.), *Proceedings of the 2023 9th International Conference on Advances in Energy Resources and Environment Engineering (ICAESEE 2023)*, Atlantis Highlights in Engineering 29,
https://doi.org/10.2991/978-94-6463-415-0_13

miy of photovoltaic power plants is reflected in the larger initial investment, longer payback period, and externally induced failure of power generation to meet expectations, which includes the PV efficiency degradation due to heat dissipation problems. Many studies have shown [2-5] that an increase in temperature will cause a decrease in the power generation efficiency of PV cells, with a decrease of approximately 0.4~0.5% in power generation efficiency for every 1K increase in temperature. In order to maintain the acceptable level of power generation efficiency, PV/T systems with cooling units that can collect solar thermal energy have been proposed and put into use.

Tripanagnostopoulos et al. [6] made contributions to water cooling research and showed that water is sufficient as a heat transfer fluid compared to air in all cases they studied. Under the same weather conditions, water cooling can keep the working temperature of the PV panel at 38℃, which is 3℃ lower than air cooling. Khanjari et al. [7] cooled PV cells using nano-fluids and proved that adding nano-materials to pure water can indeed help improve the efficiency of PV/T systems. Compared to pure water, Ag-water nanofluid can have a gain of up to 7.16% for power generation efficiency at a volume fraction of 5%. Arıcı et al. [8] used PCMs as coolant of PV panel and proved that the working temperature of PV panel reduced by up to 10.26℃ when using the suitable PCM for the PV panel for the given climatic conditions, which means a power generation efficiency gain of 3.73%. In the research made by Feng et al. [9], a dual cooling system utilizing fresh air and domestic water for indoor warm air and domestic hot water supply proved to be feasible under ideal conditions. This means that dual cooling systems can be seen as an effective way to reduce thermal loads while increasing power generation efficiency in a some area.

All of the above studies have demonstrated the necessity of cooling systems to improve PV efficiency, however, there are differences in the selection of the type and parameters of the cooling system under different climatic conditions. The system studied in this paper is a PV/T residential system that integrates air-cooling and water-cooling units. The cooling air of the air-cooling unit comes from envirnment, while the cooling water comes from a thermal buffer tank placed in the basement. Since the temperature of the cooling source is highly dependent on the climatic conditions, the same cooling system shows different environmental adaptations in different regions. This paper will investigate the electricity generation and heating performance of air-cooling, water-cooling, and dual-cooling units at different cooling fluid mass flow rates in different typical climate zones in China.

Accordingly, this paper tested the system performance under four operating scenarios, and separately calculated their electricity generation, thermal and total efficiency. The situation of four scenarios with different operational flow rates of air and water for the PV-T solar collector is shown in Table 1.

Table 1. Operational flow rates of air and water for the PV-T solar collector

Scenario	Mass flow of cooling air in kg/s	Mass flow of cooling water in kg/s
Scenario 1	0	0
Scenario 2	0.005 ~ 0.030	0
Scenario 3	0	0.005 ~ 0.030
Scenario 4	0.005 ~ 0.030	0.005 ~ 0.030

Compared to the existing research, this paper differs by focusing on the applicability of the dual cooling PV/T collector in chinese conditions, which need to provide answers to the questions of what cooling method should be adopted to enhance the collector efficiency under different climatic conditions in China, and how the size of its coolant flow rate should be selected.

2 Modeling

The mathematical modeling of the system will be presented in the form of Python code, which will be iterated at a 60-second interval to evaluate the overall performance of the PV/T system in generating electricity and providing heat throughout the year, considering the operation of the cooling units with different forms and mass flow rates.

Table 2. Climate condition of five typical cities located in different climatic zones of China

Cities	Optimal tilted angle	PV generator working			Annual average situation		
		GTI in W/m^2	T_A in °C	v_w in m/s	GTI in W/m2	T_A in °C	v_w in m/s
Beijing	35°	384.32	17.54	3.08	181.00	13.28	2.82
Hangzhou	20°	308.62	20.68	2.62	144.69	18.09	2.46
Lhasa	15°	535.12	13.69	2.29	257.83	9.98	1.80
Sanya	37°	422.89	26.13	3.99	200.89	24.85	3.56
Urumqi	35°	409.33	12.87	2.80	191.02	8.37	2.36

The meteorological data used in this study are obtained from Meteonorm 8, including global tilted irradiation (GTI), ambient temperature (TA), and wind speed (vw). It is worth noting that the optimal tilt angle of solar collector varies with latitude and climate. In this study, some researches [10-12] has been refered and the tilt angles that maximize the solar radiation intensity for five typical cities in different climatic regions of China has been confirmed. The details are shown in Table 2.

2.1 Structure of PV/T system

This paper presents a PV/T system that integrates air-cooling and water-cooling units on the collector, whose structure is shown in Fig.1. In the PV/T system, the battery circuit is used to collect and store the electricity generated by PV cells through the photoelectric effect. The air-cooling and water-coole units respectively use the outside air (fresh air from environment) and water stored in the thermal buffer tank to cool the PV cells. The PV cells that complete the cooling process have lower temperature compared to before, which allows them to maintain a higher power generation efficiency. The air that has completed heat exchange will be discharged from the system by the air pump, while the water that has completed heat exchange will be transported to the designated water layer in the thermal buffer tank through the temperature stratifier and the water pump. The hot water stored in the top water layer of the storage tank will

heat the domestic water in the plate heat exchanger and thereby lowering its own temperature. Whether air-cooling or water-cooling, the coolant needs to be drived by circulation pump. Predictably, because air is less dense than water, an air circulation pump with the same flow rate will have lower power consumption than a water circulation pump when they are installed in close position.

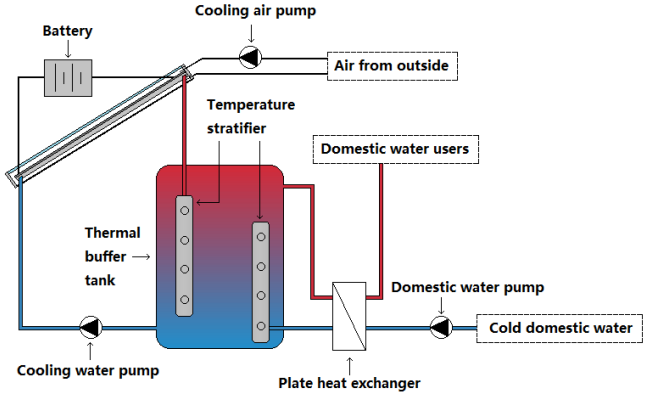

Fig. 1. Structure of PV/T system with integrated air and water cooling units

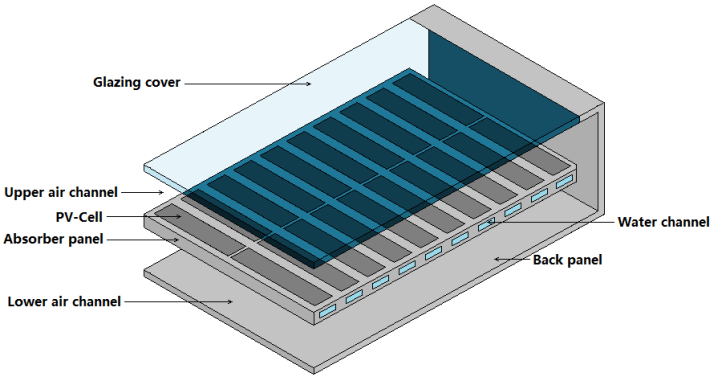

Fig. 2. Structure of PV/T collector with integrated air and water cooling unit

The structure of PV/T collector with integrated dual cooling unit is shown in Fig.2. As shown in the figure, the glazing cover and back panel sandwich the PV cell and absorber panel, with gaps between them forming upper and lower separated but interconnected air-cooling channels. Cooling air enters from the upper air channel and exits from the lower air channel. The control logic is to turn on the air-cooling pump when the temperature of the cooling air is 2K or more lower than that of the PV cell, and turn it off when the temperature is higher. A water channel is also set up in the absorber panel to allow cooling water to enter for water-cooling the PV cell. The control logic is to turn on the water-cooling device when the temperature of the cooling water is 5K or more lower than that of the PV cell, and turn it off when the temperature difference is smaller than this threshold value.

2.2 Mathematical Modeling

The energy flow in the above PV/T collector is shown in Fig.3. The meanings of the lower corner marker and symbols that appear in the following mathematical modeling are summarized in Table 3 and Table 4.

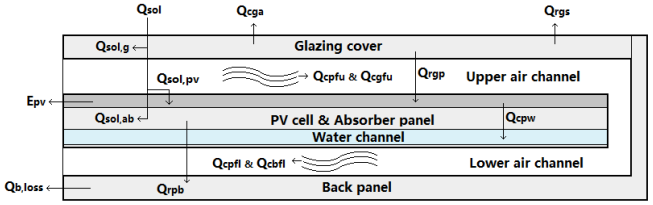

Fig. 3. Energy flow in PV/T collector with integrated air and water cooling units

Table 3. Meanings of lower corner markers in mathematical modeling

Markers	Meaning	Markers	Meaning
c	Convection heat transfer	a, ab	Absorber panel
r	Radiant heat exchange	f	Air in air channel
sol	Solar irradiation	C	Solar collector
g	Glazing cover	w	Fluid in water channel
p, pv	PV cell	b	Back panel

Table 4. Meanings of symbols in mathematical modeling

Symbol	Meaning	Unit	Symbol	Meaning	Unit
q	Heat flow	W	I	Irradiance intensity	W/m^2
c	Specific heat capacity	J/(kg·K)	α	Absorptivity	-
m	Mass flow	kg/s	ε	Emissivity	-
h	Convective heat transfer coefficient	$W/(m^2 \cdot K)$	σ	Stefan-Boltzmann constant	$W/(m^2 \cdot K^4)$
A	Area	m^2	τ	transmittance	-
T/t	Temperature	K/°C	v	Wind speed	m/s
μ	dynamic viscosity	Pa·s	E	PV electricity	W
Nu	Nusselt number	-	D_H	equivalent diameter	m
Re	Reynolds number	-	η	Efficiency	%
Pr	Prandtl number	-	F_{ab}	Efficiency of collector	%
W	Width of the channel	m	U	Heat transfer coefficient	$W/(m^2 \cdot K)$
d	Depth of the channel	m	L	Length of the channel	m

Glazing cover. The mathematical modeling of energy flow related to the glazing cover is as follows:

$$c_g \cdot m_g \cdot \frac{dT_g}{dt} = q_{sol,g} - q_{rgp} - q_{rgs} - q_{cga} - q_{cgfu} \tag{1}$$

$$\mathrm{q_{sol,g}} = \mathrm{I_{sol}} \cdot \alpha_\mathrm{g} \cdot \mathrm{A_c} \tag{2}$$

$$\mathrm{q_{rgp}} = h_\mathrm{rgp} \cdot \mathrm{A_{ab}} \cdot (\mathrm{T_g} - \mathrm{T_{pv}}) \tag{3}$$

[13]
$$h_\mathrm{rgp} = \frac{\sigma(\mathrm{T_{pv}} + \mathrm{T_g})(\mathrm{T_{pv}^2} + \mathrm{T_g^2})}{\frac{1}{\varepsilon_\mathrm{pv}} + \frac{1}{\varepsilon_\mathrm{g}} - 1} \tag{4}$$

$$\mathrm{q_{rgs}} = h_\mathrm{rgs} \cdot (\mathrm{T_g} - \mathrm{T_s}) \cdot \mathrm{A_c} \tag{5}$$

[14]
$$h_\mathrm{rgs} = \sigma \cdot \varepsilon_\mathrm{g} \cdot (\mathrm{T_g^2} + \mathrm{T_s^2})(\mathrm{T_g} + \mathrm{T_s}) \tag{6}$$

[15]
$$\mathrm{T_s} \approx 0.0552 \cdot \mathrm{T_a^{1.5}} \tag{7}$$

$$\mathrm{q_{cga}} = h_\mathrm{cga} \cdot (\mathrm{T_g} - \mathrm{T_a}) \cdot \mathrm{A_c} \tag{8}$$

[16]
$$h_\mathrm{cga} = 3.8 \cdot \mathrm{v} + 5.7 \tag{9}$$

$$\mathrm{q_{cgfu}} = h_\mathrm{cgfu} \cdot (\mathrm{T_g} - \mathrm{T_{fu}}) \cdot \mathrm{A_c} \tag{10}$$

$$h_\mathrm{cgfu} = \frac{\mathrm{Nu_{fu}} \cdot \lambda_\mathrm{fu}}{\mathrm{D_{H,fu}}} = \frac{\mathrm{Nu_{fu}} \cdot \lambda_\mathrm{fu} \cdot 2 \cdot (\mathrm{W} + \mathrm{d})}{4 \cdot \mathrm{W} \cdot \mathrm{d}} \tag{11}$$

$$\mathrm{Re} = \frac{\dot{m}_\mathrm{fu} \cdot \mathrm{D_{H,fu}}}{\mathrm{A_{fu}} \cdot \mu_\mathrm{fu}} \tag{12}$$

However, different researchers have provided different answers regarding the critical Reynolds number between different flow states [17-20]. This paper adopts the method of Bergman et al. in their work [20] to solve the Nusselt number, using Re=2300 and Re=6000 as standards to distinguish different flow states. The value of Nu is obtained by using the Prandtl number and Reynolds number together:

$$\mathrm{Pr} = \frac{\mathrm{C_{p,fu}} \cdot \mu_\mathrm{fu}}{\lambda_\mathrm{fu}} \tag{13}$$

Therefore, the Nusselt number of the fluid in the upper air channel is:

①When Re < 2300, the flow state of fluid is laminar flow:

$$\mathrm{Nu_{fu}} = 5.4 + \frac{0.0019 \cdot \left[\mathrm{Re} \cdot \mathrm{Pr} \cdot (\frac{\mathrm{D_{H,fu}}}{\mathrm{L}})\right]^{1.71}}{1 + 0.00563 \cdot \left[\mathrm{Re} \cdot \mathrm{Pr} \cdot (\frac{\mathrm{D_{H,fu}}}{\mathrm{L}})\right]^{1.17}} \tag{14}$$

②When 2300 < Re < 6000, the flow state of fluid is transitional flow:

$$\mathrm{Nu_{fu}} = 0.116 \cdot (\mathrm{Re}^{\frac{2}{3}} - 125) \cdot \mathrm{Pr}^{\frac{1}{3}} \cdot [1 + (\frac{\mathrm{D_{H,fu}}}{\mathrm{L}})^{\frac{2}{3}}] \cdot (\frac{\mu_\mathrm{fu}}{\mu_\mathrm{w}})^{0.14} \tag{15}$$

③When Re > 6000, the flow state of fluid is turbulent flow:

$$\mathrm{Nu_{fu}} = 0.018 \cdot \mathrm{Re}^{0.8} \cdot \mathrm{Pr}^{0.4} \tag{16}$$

PV cell and absorber panel. It is assumed that the temperature of the absorber panel is always the same as that of the PV cell, and their characteristics in heat exchange process can be approximated to be the same as those of the PV cell. Under this premise, the mathematical modeling of energy flow related to the PV cell and absorber panel is as follows:

$$\mathrm{c_{pv}} \cdot \mathrm{m_{pv}} \cdot \frac{\mathrm{dT_{pv}}}{\mathrm{dt}} = \mathrm{q_{sol,pv+ab}} - \mathrm{E_{pv}} + \mathrm{q_{rgp}} - \mathrm{q_{cpfu}} - \mathrm{q_{cpw}} - \mathrm{q_{cpfl}} - \mathrm{q_{rpb}} \tag{17}$$

$$\mathrm{q_{sol,pv+ab}} = \mathrm{q_{sol,pv}} + \mathrm{q_{sol,ab}} = \mathrm{I_{sol}} \cdot \tau_\mathrm{g} \cdot [\alpha_\mathrm{pv} \cdot \mathrm{A_{pv}} + \alpha_\mathrm{ab} \cdot (\mathrm{A_{ab}} - \mathrm{A_{pv}})] \tag{18}$$

[21]

$$E_{pv} = q_{sol,pv} \cdot \eta_{pv} \cdot (1 - \theta_{pv} \cdot (T_p - 298.15)) \quad (19)$$

$$q_{cpw} = h_{cpw} \cdot A_{ab} \cdot (T_p - T_w) \quad (20)$$

$$h_{cpw} = \frac{Nu_w \cdot \lambda_w}{D_{H,w}} \cdot F_{ab} \quad (21)$$

$$q_{cpf} = h_{cpf} \cdot A_{ab} \cdot (T_p - T_f) \quad (22)$$

$$h_{cpf} = \frac{Nu_f \cdot \lambda_f}{D_{H,f}} \quad (23)$$

$$q_{rpb} = h_{rpb} \cdot A_{ab} \cdot (T_{pv} - T_b) \quad (24)$$

$$h_{rpb} = \frac{\sigma(T_{pv} + T_b)(T_{pv}^2 + T_b^2)}{\frac{1}{\varepsilon_{pv}} + \frac{1}{\varepsilon_b} - 1} \quad (25)$$

Upper and lower air channels, water channel and back panel. Mathematical models describing the energy flow related to the upper and lower air channels, water channel, and back panel can be respectively described by the following four equations:

$$c_{fu} \cdot m_{fu} \cdot \frac{dT_{fu}}{dt} = q_{cpfu} + q_{cgfu} \quad (26)$$

$$c_{fl} \cdot m_{fl} \cdot \frac{dT_{fl}}{dt} = q_{cbfl} + q_{cpfl} \quad (27)$$

$$c_w \cdot m_w \cdot \frac{dT_w}{dt} = q_{cpw} \quad (28)$$

$$c_b \cdot m_b \cdot \frac{dT_b}{dt} = q_{rpb} - q_{cbfl} - U_b \cdot A_c \cdot (T_b - T_a) \quad (29)$$

It should be noted that the density, specific heat capacity, thermal conductivity, and viscosity of the cooling fluid will vary with temperature. In this paper, the influence of temperature changes on the above four physical quantities of air (-20~125℃) and water (0~100℃) was quantified by polynomial fitting, and the results are summarized in Table 5 and Table 6.

Table 5. The relationship between the thermophysical parameters of air and temperature

Parameters	Mathematical fitting result
Density (kg/m^3)	$5.5962 - 0.035153T_f + 0.000109T_f^2 - 1.696546 \times 10^{-7}T_f^3 + 1.044189 \times 10^{-10}T_f^4$
Heat Capacity (J/kg·K)	$1029.2 - 0.192610T_f + 0.000413T_f^2 - 1.407906 \times 10^{-7}T_f^3 + 1.939579 \times 10^{-10}T_f^4$
Thermal Conductivity (W/m·K)	$-0.0021 + 0.000119T_f - 9.702624 \times 10^{-8}T_f^2 + 5.398308 \times 10^{-11}T_f^3 - 5.250589 \times 10^{-15}T_f^4$
Viscosity (Pa·s)	$-1.00377 \times 10^{-6} + 9.053724 \times 10^{-8}T_f - 1.153283 \times 10^{-10}T_f^2 + 1.188221 \times 10^{-13}T_f^3 - 5.610924 \times 10^{-17}T_f^4$

Table 6. The relationship between the thermophysical parameters of water and temperature

Parameters	Mathematical fitting result
Density (kg/m^3)	$-994.8571 + 22.154508T_w - 0.090803T_w^2 + 0.000165T_w^3 - 1.154737 \times 10^{-7}T_w^4$
Heat Capacity (J/kg·K)	$35861.1475 - 375.799709T_w + 1.674767T_w^2 - 0.003327T_w^3 + 2.489017 \times 10^{-6}T_w^4$
Thermal Conductivity (W/m·K)	$6.5179 - 0.082622T_w + 0.000407T_w^2 - 8.551584 \times 10^{-7}T_w^3 + 6.554167 \times 10^{-10}T_w^4$
Viscosity (Pa·s)	$0.4583 - 0.005302T_w + 2.311436 \times 10^{-5}T_w^2 - 4.490993 \times 10^{-8}T_w^3 + 3.277589 \times 10^{-11}T_w^4$

Thermal buffer tank. Due to the installation of a temperature stratifier in the water tank, there exists a vertical temperature gradient in different water layers, with the highest temperature at the top and the lowest temperature at the bottom, and heat exchange occurs among different water layers. Finite Element Analysis (FEA) is used here to simulate the heat flow inside the water tank, and the temperature at 5 outlets located at 10%, 30%, 50%, 70% and 90% of tank height is determined respectively. The water tank will supply heat to domestic hot water only when the temperature of the water layer at 90% of the tank height is 5K higher than domestic hot water.

Modeling parameters. Values of the design parameters, constants and ambient conditions used in the modeling is shown in Table 7.

Table 7. Values of the design parameters, constants and ambient conditions

Parameters		Value	Parameters		Value
Area of single collector	A_C	2 m^2	Thickness of PV cell	h_{pv}	0.004 m
Area of single absorber panel	A_{ab}	1.872 m^2	Thickness of glazing cover	th_g	0.004 m
Area of single PV cell	A_{pv}	1.752 m^2	Absorptivity of PV cell	A_{pv}	0.85
Upper channel depth	d_{fu}	0.07 m	Absorptivity of glazing cover	α_g	0.05
Lower channel depth	d_{fl}	0.04 m	PV cell efficiency (in 25°C)	Θ_{pv}	15 %
Tube hydraulic diameter	$D_{H,w}$	0.0158 m	Transmissivity of glazing cover	τ_g	0.95
Emissivity of glazing cover	ε_g	0.85	Temperature coefficient	β_{pv}	0.45 %/K

System efficiency. The definition of system efficiency is not uniform. In this study, the definition of system efficiency is the ratio of the total electricity or total heat supplied to the user to the total solar energy absorbed by the PV/T collector. Therefore, the power generation efficiency η_{el}, thermal efficiency η_{th}, and overall efficiency η_{tot} of the PV/T system can be expressed as:

$$\eta_{tot} = \eta_{el} + \eta_{th} = \eta_{pv} \cdot (1 - \theta_{pv} \cdot (T_p - 298.15)) \cdot \eta_{ppt} + \frac{q_{ctdw}}{I_{sol} \cdot \tau_g \cdot [\alpha_{pv} \cdot A_{pv} + \alpha_{ab} \cdot (A_{ab} - A_{pv})]} \quad (30)$$

3 Data analysis

As shown in Fig 4, due to the significant deviation between the real-world environment and laboratory conditions, the efficiency of a PV cell without any cooling unit installed is far from the reference level of 15%.

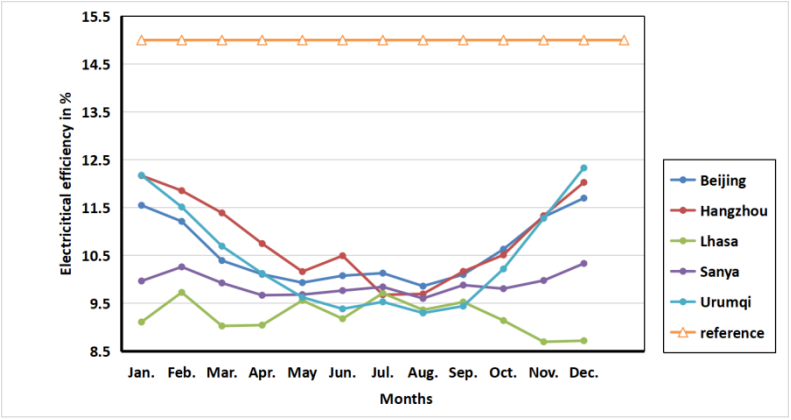

Fig. 4. Variation of the annual average power generation efficiency of PV cells without cooling

It is noteworthy that for PV cells without cooling units, the impact of the increase in solar radiation intensity on their efficiency is more critical than that of the rise in ambient temperature. This is because the ambient temperature mainly contributes to the heat exchange of the glazing cover, while the PV cell can only rely on its own radiative heat exchange with the surroundings (environment). This leads to the fact that when PV cells are in operation, the efficiency of the PV cell placed in Beijing (with an average ambient temperature of about 28.87℃ and solar radiation intensity of about 360.88W/m^2 in August) is 0.50% higher than that placed in Lhasa (with an average ambient temperature of about 19.16℃ and solar radiation intensity of about 454.79W/m^2 in August). Therefore, the demand for cooling units in areas with strong radiation intensity, such as alpine and tropical monsoon climate zones, is much higher than in other climatic zones.

Moreover, due to the difference in the thermal properties of land and sea, continental and monsoon climates not only have differences in precipitation but also have distinct differences in temperature distribution. In areas where there is no ocean, the average temperature difference between winter and summer is large, and the temperature changes faster throughout the day. These factors jointly lead to the fact that the demand for cooling in PV cells installed in continental climate zones is higher in summers than in monsoon climate zones, while their cooling demand is relatively low in winters. For this reason, PV cells installed in Urumqi have the lowest efficiency in summers among

all regions, while Beijing, located in a temperate monsoon climate zone, relies on its relatively low average temperature and small winter-summer temperature difference, showing relatively high efficiency throughout the year.

3.1 Air-cooling PV/T system

Fig.5 summarizes the variation of the annual average efficiency of a air-cooling photovoltaic system with changes in the cooling air flow rate. The x-axis represents the mass flow rate of air in kg/s, while the y-axis represents the power generation efficiency of the PV panel. As the flow rate increases, the efficiency gain caused by air cooling exhibits nonlinear characteristics and gradually show marginal effects. Moreover, at a mass flow rate of 0.025 kg/s, the annual average efficiency is almost the same as that at 0.01 kg/s. In most cases, this difference is about 0.6%. The reason for this phenomenon is that the generation of complex three-dimensional flows leads to the fact that the Nusselt number does not increase monotonically with an increase in the Reynolds number [22]. But it should be noted that this explanation is not suitable in all sizes of equipment.

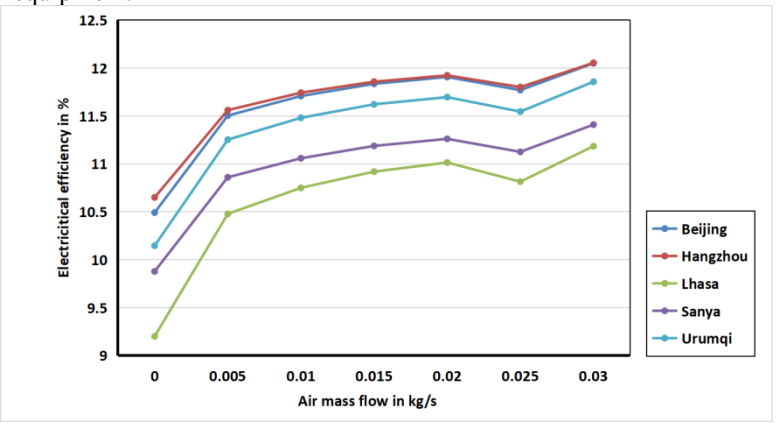

Fig. 5. Variation of the annual average power generation efficiency of air-cooling PV cells with cooling air mass flow

Compared to a PV cell without cooling, the annual average power generation efficiency of air-cooling PV cells installed in various climatic zones has been greatly improved. Among them, the air-cooling unit has the best gain effect in high-altitude mountainous climate zones, the power generation efficiency increases from 9.20% to 11.18% with the gradual increase in flow rate. The second place goes to the temperate continental climate zone represented by Urumqi, whose efficiency also increased from 10.15% to 11.86%. For other regions, the maximum increase in generating efficiency due to air-cooling units is in the range of 1.4% to 1.55%. The reason for this phenomenon is that the annual average temperature in these regions is lower, which is more conducive to the role of air cooling. On the contrary, as the temperature rises, the air cooling effect decreases, and therefore, the air cooling gain in Sanya, located in a tropical region, is the worst.

Fig 5 also shows some noteworthy information. Under all cooling air flow rates, Hangzhou, which ranks second in terms of average temperature among the five cities, has the highest annual average photovoltaic power generation efficiency, as the solar radiation intensity in this region is the lowest. Because Hangzhou is located in a subtropical region with high air humidity, and these water vapor and aerosols affect the amount of solar radiation that can be received on the ground surface [23]. In addition, its latitude is not low enough to enjoy longer sunlight hours and stronger light intensity like tropical monsoon climate cities such as Sanya. Therefore, although it has a higher PV power generation efficiency, its power generation capacity is the lowest among all climatic zones. More details are shown in Table 8, from which it can be seen that for high-radiation regions such as Lhasa and Urumqi, although the power generation efficiency is not excellent, their PV power generation capacity still ranks first.

Table 8. Annual power production at different air flow rates in different climate zones

Cities	Annual power production of PV cell at different air flow rates in kWh/m^2					
	0.005 kg/s	0.010 kg/s	0.015 kg/s	0.020 kg/s	0.025 kg/s	0.030 kg/s
Beijing	132.01	134.36	135.82	136.64	135.06	138.28
Hangzhou	106.27	107.94	109.00	109.60	108.48	110.81
Lhasa	171.18	175.62	178.38	179.93	176.67	182.71
Sanya	138.36	140.88	142.53	143.47	141.74	145.35
Urumqi	136.24	139.00	140.70	141.61	139.78	143.55

In summary, for areas with high temperatures, the mass flow rate and size of the air-cooling unit should be considered when selecting the system, and blindly choosing the highest specification may not be economical. On the other hand, for areas with lower temperatures, the selection of air-cooling unit can be configured towards high specifications as the gains are relatively greater.

3.2 Water-cooling PV/T system

Impact on power generation efficiency. The variation of the annual average power generation efficiency of water-cooling PV cells with cooling water mass flow is summarized in Fig.6. The x-axis represents the mass flow rate of water in kg/s, while the y-axis represents the power generation efficiency of the PV panel. As shown in the figure, with the increase of cooling water mass flow rate, the efficiency gain caused by water cooling exhibits a monotonic non-linear characteristic, which is unlike the air-cooling system. The efficiency gain brought by the water-cooling system is much greater than that of the air-cooling system. In Lhasa, for instance, when the water-cooling system is installed and cooled with a low mass flow rate of 0.005kg/s, the solar energy efficiency gain is about 3.72%. Compared to air-cooling, even with a large flow rate of 0.03kg/s, the air-cooling system can bring about a gain of about 1.98% in solar energy efficiency. However, marginal effects still remain, which result in a power generation efficiency improvement of less than 0.04% for most areas when the water flow rises from 0.025kg/s to 0.03kg/s.

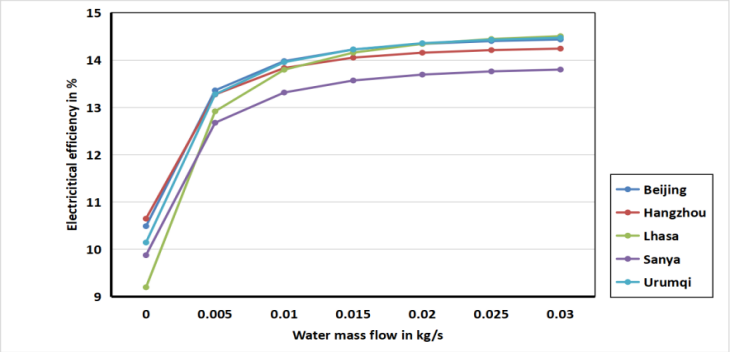

Fig. 6. Variation of the annual average power generation efficiency of water-cooling PV cells with cooling water mass flow

From the perspective of the environmental adaptability of the water-cooling system, Lhasa still shows its best performance. With the increase of cooling water mass flow rate, the power generation efficiency in this region has increased from the lowest 9.20% of 14.51%. The reason for this phenomenon is that the ambient temperature in Lhasa is not high, and the temperature of cold domestic water is low enough, which causes the water in the tank to be exothermic for a longer period of time. Therefore, the cooling effect of the water-cooling system is guaranteed. On the contrary, the effect of the water-cooling system in the tropical monsoon zone is relatively worse than that in other climate zones because the higher environmental temperature brings a higher domestic water temperature, and the water temperature in the tank is in a "high temperature" state for a long time, which limits the cooling effect of the water-cooling system. However, unlike the air-cooling system, the water-cooling system, when put into operation, allows the power generation efficiency in high-radiation areas to exceed that in low-radiation areas, provided that the temperature of domestic water (strong correlation with ambient temperature) is low enough. The power generation of water-cooling PV/T systems in cities with different climate is shown in Table 9.

Table 9. Annual power production of water-cooling PV/T system at different water flow rates in different climate zones

Cities	Annual power production of PV/T at different water flow rates in kWh/m^2					
	0.005 kg/s	0.010 kg/s	0.015 kg/s	0.020 kg/s	0.025 kg/s	0.030 kg/s
Beijing	153.32	160.42	163.24	164.59	165.28	165.66
Hangzhou	122.01	127.17	129.18	130.13	130.64	130.93
Lhasa	211.03	225.39	231.29	234.31	236	236.98
Sanya	161.49	169.64	172.88	174.46	175.33	175.82
Urumqi	160.75	168.96	172.21	173.82	174.7	175.22

In summary, the water-cooling system is a system that is highly sensitive to environmental temperature, more precisely, this strong correlation is mainly due to the influence of air temperature on the domestic water temperature. However, the source of

domestic water in different cities is different, which may result in this strong correlation not being particularly reliable:

- Hypothesis 1: domestic water comes from surface water sources: The water temperature of residents in these cities is strongly tied to air temperature. Therefore, in these cities, lower air temperatures will make the water-cooling system play an especially positive role in improving the photovoltaic power generation efficiency.

- Hypothesis 2: domestic water comes from the South-to-North Water Diversion or underground water: The water temperature of residents in these cities is not bound to air temperature. In this case, lower air temperatures will not make the water-cooling system perform much better than higher air temperatures.

As mentioned earlier, this article adopts the first hypothesis. If the actual situation is the second hypothesis, other models need to be used for prediction.

Impact on thermal and total efficiency. Fig.7 shows the thermal efficiency of water-cooling systems at different water flow rates in cities with different climate. The water-cooling system has shown high adaptability in most regions. When the water flow rate reaches 0.030kg/s, the thermal efficiency in most regions reached over 60%. In tropical monsoon climate areas (Sanya), where the photovoltaic power generation efficiency is poor, its performance in thermal efficiency is leading other regions (68.5%). However, in the temperate continental climate zone represented by Urumqi, the thermal efficiency is lower than that of other climate zones. The reason for this is that the winter temperature in this climate zone is extremely low, and assuming that the domestic water comes from surface water sources, the low temperature makes it impossible to deliver the water to residents without preheating. According to relevant encoding standard [24], the domestic water needs to be heated before it is delivered to the storage tank near the heating source for further heating, which reduces the heating demand for the PV/T system, and results in excessive heat absorption by the storage tank without consumption. Therefore, a optimization measure is to reduce the cooling water flow rate during the cold season in the continental climate zone to save electricity when the circulating pump is running. The heating output and the annual total efficiency of water-cooling PV/T systems in different regions are shown in Table 10 and Table 11, respectively.

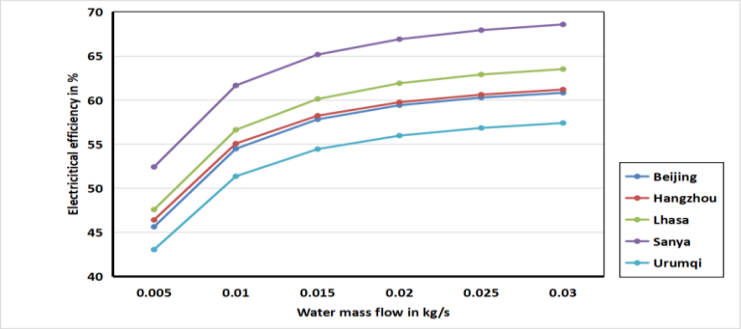

Fig. 7. Variation of the annual average thermal efficiency of water-cooling PV cells with cooling water mass flow

Table 10. Annual thermal production of water-cooling PV/T system at different water flow rates in different climate zones

Cities	Annual thermal production of PV/T at different water flow rates in GJ/m2					
	0.005 kg/s	0.010 kg/s	0.015 kg/s	0.020 kg/s	0.025 kg/s	0.030 kg/s
Beijing	1.886	2.251	2.389	2.455	2.491	2.513
Hangzhou	1.536	1.823	1.927	1.978	2.006	2.025
Lhasa	2.799	3.331	3.536	3.641	3.699	3.736
Sanya	2.405	2.828	2.989	3.069	3.116	3.145
Urumqi	1.877	2.239	2.373	2.440	2.478	2.502

Table 11. Annual total efficiency of water-cooling PV/T system at different water flow rates in different climate zones

Cities	Annual total efficiency of water-cooling PV/T system in %					
	0.005 kg/s	0.010 kg/s	0.015 kg/s	0.020 kg/s	0.025 kg/s	0.030 kg/s
Beijing	59	68.47	72.05	73.76	74.69	75.26
Hangzhou	59.7	68.91	72.29	73.91	74.83	75.44
Lhasa	60.51	70.43	74.29	76.25	77.35	78.02
Sanya	65.11	74.98	78.73	80.6	81.69	82.38
Urumqi	56.34	65.32	68.67	70.33	71.27	71.88

3.3 Dual-cooling PV/T system

Impact on thermal and total efficiency. Fig.8 and Fig.9 show the annual average power generation efficiency and its absolute increase (compare with air-cooling unit) of the dual-cooling PV/T device with air mass flow rate of 0.01 kg/s and 0.03 kg/s vary with the cooling water mass flow rate, respectively.

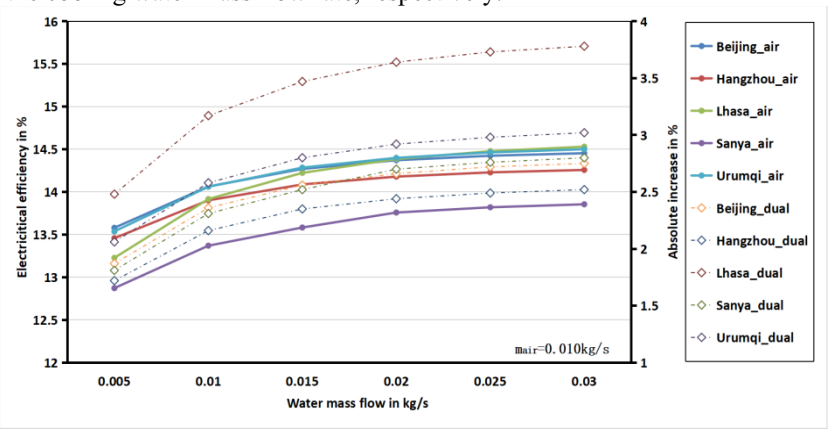

Fig. 8. The annual average power generation efficiency and its absolute increase of the dual-cooling PV/T device with air mass flow rate of 0.01 kg/s vary with water flow rate

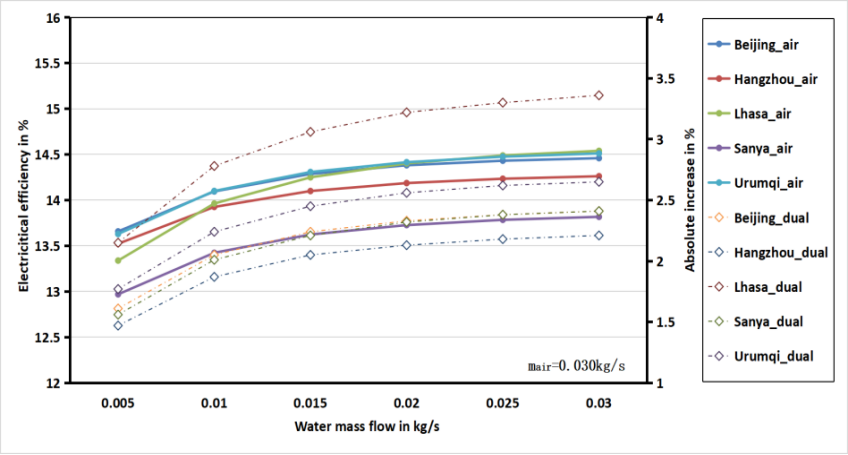

Fig. 9. The annual average power generation efficiency and its absolute increase of the dual-cooling PV/T device with air mass flow rate of 0.03 kg/s vary with water flow rate

Based on the figure shown, integrating a water-cooling unit into a PV/T system that was originally equipped with a single air-cooling unit will greatly improve the PV power generation efficiency, regardless of the size of the original air-cooling flow rate. For instance, in Lhasa, when both air and water flow rates are 0.03kg/s, the absolute increase in power generation efficiency compared to a single air-cooling PV/T system can reach 3.36%. Even in Hangzhou, which performed slightly worse, the increase reached 2.21% under the same cooling unit parameters. Thus, it can be concluded that the dual-cooling system will bring significant efficiency gains to a single air-cooling PV/T device.

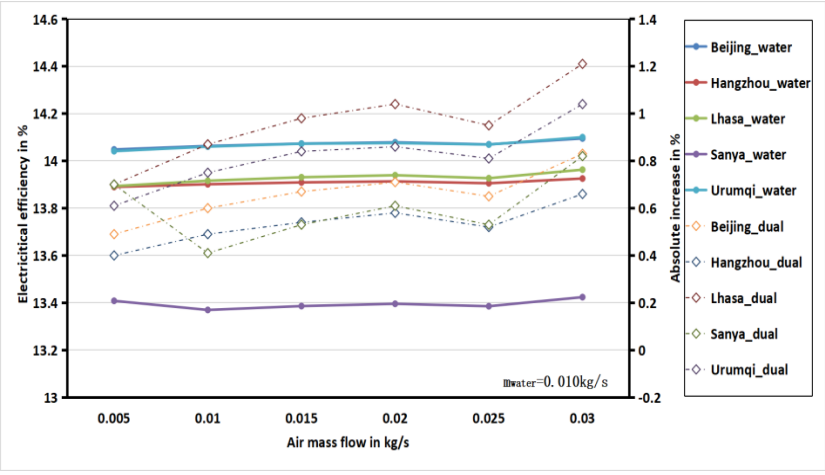

Fig. 10. The annual average power generation efficiency and its absolute increase of the dual-cooling PV/T device with water mass flow rate of 0.01 kg/s vary with air flow rate

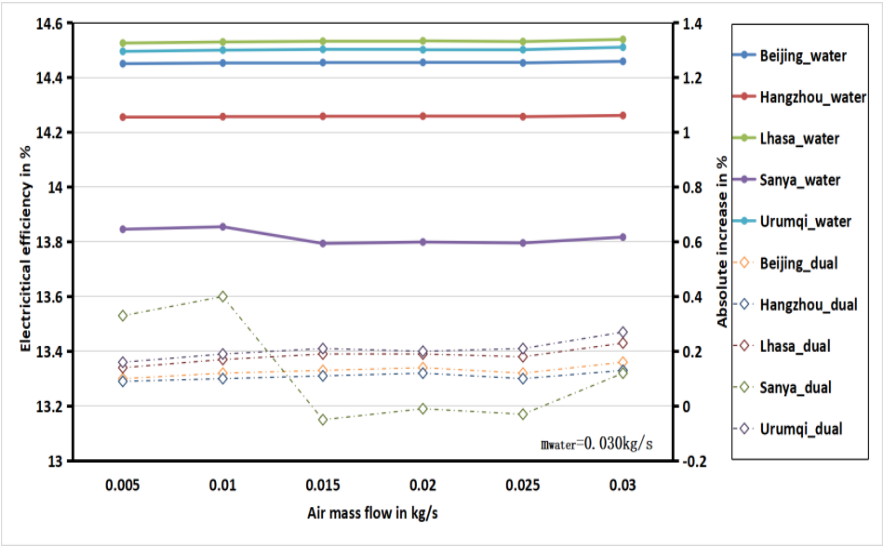

Fig. 11. The annual average power generation efficiency and its absolute increase of the dual-cooling PV/T device with water mass flow rate of 0.03 kg/s vary with air flow rate

Fig.10 and Fig.11 show the annual average power generation efficiency and its absolute increase of the dual-cooling PV/T device with water mass flow rate of 0.01 kg/s and 0.03 kg/s vary with the cooling air mass flow rate, respectively. As shown in Fig.10, the dual-cooling system does result in power generation efficiency gains compared to the low-flow water-cooling system, e.g., when the water and air flow rate are 0.01 kg/s and 0.03 kg/s, the efficiency gains for the PV panel in Lhasa, Urumqi, Beijing, Sanya and Hangzhou are 1.21%, 1.04%, 0.83%, 0.82% and 0.66%, respectively. However, when the water flow rate becomes larger, dual-cooling is not recommended. As shown in Fig.11, in the Sanya, when the water flow rate is 0.03 kg/s, accompanied by the rise of the cooling air volume within a certain range (0.015~0.025 kg/s), the power generation efficiency shows a small decrease compared to the water-cooling system, which is due to the fact that in this range, the period that the temperature difference between the PV panel and the cooling water is less than 5 K becomes longer, which makes the turn-on time of the water-cooling system to be shortened, and when the flow rate is further increased, air takes away more heat, while at the same time, it does not shorten the turn-on time of the water-cooling system any further, so the efficiency shows a small recovery.

Impact on thermal and total efficiency. Fig.12 and Fig.13 show the annual average thermal efficiency and its absolute increase (compare with water-cooling unit) of the dual-cooling PV/T device with water mass flow rate of 0.01 kg/s and 0.03 kg/s vary with the cooling air mass flow rate, respectively.

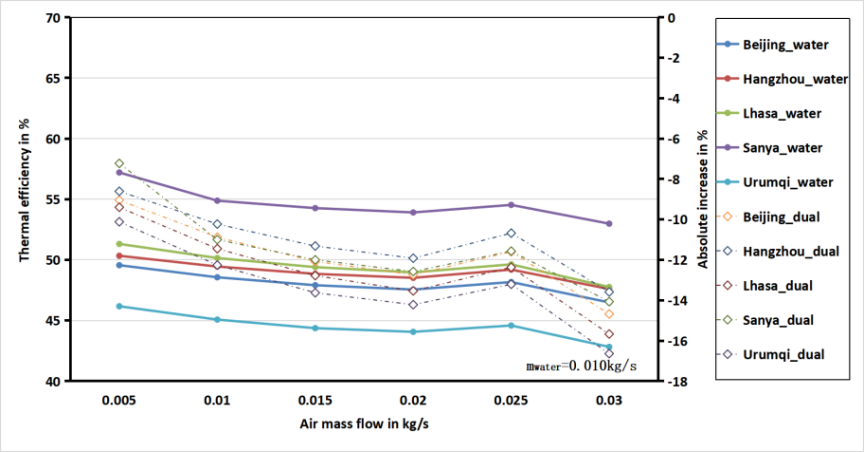

Fig. 12. The annual average thermal efficiency and its absolute increase of the dual-cooling PV/T device with water mass flow rate of 0.01 kg/s vary with air flow rate

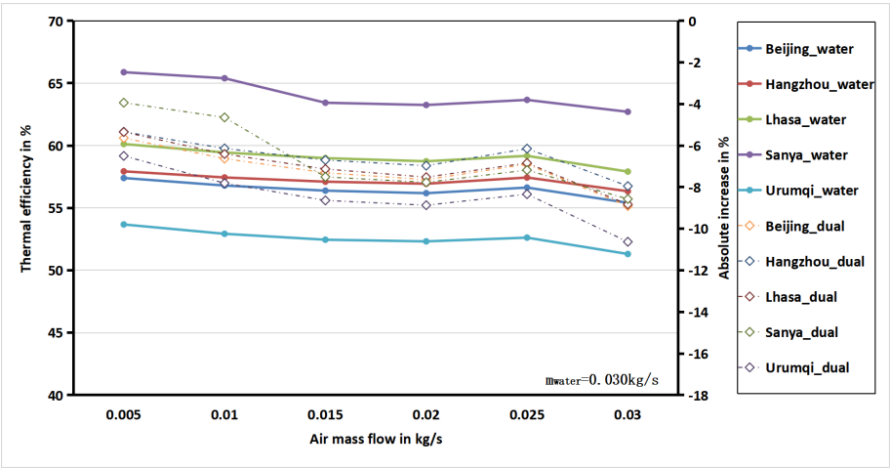

Fig. 13. The annual average thermal efficiency and its absolute increase of the dual-cooling PV/T device with water mass flow rate of 0.03 kg/s vary with air flow rate

As shown in the figure, when an air-cooling unit is integrated into a single water-cooling PV/T system, the thermal efficiency will decrease regardless of the airflow rate setting. This decrease in thermal efficiency is much greater than the increase in PV power generation efficiency that the air-cooling unit brings. For example, in Lhasa, when the mass flow rates of both air and cooling water are 0.03kg/s and 0.01kg/s, respectively, the maximum increase in PV power generation efficiency is 1.21%. However, at the same time, the thermal efficiency drops by 15.67%. Although the above situation is slightly alleviated at a water flow rate of 0.03 kg/s, the loss in heating efficiency still generally reaches 8%. For the most part, it's more than worth it.

4 Conclusion

Air-, water-, and dual-cooling units are all effective in reducing the temperature of PV cells during operation, thereby increasing their efficiency. In most cases, a single air-cooling unit is weaker in improving PV efficiency than a single water-cooling unit, which in turn is weaker than a dual-cooling unit. However, when deciding which cooling unit to install and how to set its parameters, it is important to take into account the climatic conditions of different regions, as this can greatly affect system performance:

(1) High-flow air-cooled units can provide PV panels with a power generation efficiency of more than 1.5%, a figure that can reach close to 2% for regions with good passive cooling conditions (low ambient temperature). In addition due to thecomplex three-dimensional flows, its design requires careful consideration of the Air channel size to prevent the heat transfer efficiency of the air cooling from being lower than expected. Overall, the air-cooled system has a limited cooling capacity, so it is economically competitive only because of its lower energy consumption.

(2) Water-cooled units are the best for total PV/T collector efficiency, and in all regions, high-flow water-cooled units can guarantee a total efficiency higher than 71%, and in the best-performing regions (high radiation and high ambient temperature), this figure can reach 82.38%. However, it should be noted that the thermal efficiency of the water-cooled units has a strong correlation with the temperature of the water source used for residential water, so that when the temperature of the water source is too low (which needs to be preheated before reaching the residential user) or too high, the effect is lower than expected.

(3) In most cases, the dual cooling unit is the best of the three for PV/T collector power generation efficiency, but this is based on the premise that more low-temperature heat is wasted. In addition, due to the mismatch of control logic, the water-cooled cycle may be restricted from starting because the control temperature difference is not reached. For the adjustment of the control logic, it should be noted that, if the temperature difference requirement for the water-cooled cycle to turn on is reduced, the energy of the water-circulation pump may be wasted, and if the temperature difference requirement for the air-cooled cycle to turn on is increased, the air-cooled cycle may not be able to perform at its optimal effect. These issues are more related to the temperature of the air and residential water sources and need to be fully considered in the design.

For the future research direction of the dual-cooling system, the matching of control logic is a good research direction, how to control the opening of the two cooling cycles through the appropriate algorithms according to the changes of environmental condition, so that the cooling effect of both can be maximized.

Declarations

The authors declare that they have no competing interests. The datasets used or analysed during the current study are available from the corresponding author on reason-

able request. There is no funding for this research. A preprint has previously been published[25].

Reference

1. Zhi Q, Sun H, Li Y, et al.: China's solar photovoltaic policy: An analysis based on policy instruments. Applied Energy 129, 308-319(2014).
2. Kazem H, Chaichan M: Effect of environmental variables on PV performancebased on experimental studies. IJCMES 2(4), 1-8(2016).
3. Gasparin F, Buhler A, Rampinelli G, Krenzinger A: Statistical analysis of I–V curve parameters from PV modules. Sol Energy 131, 30-38(2016).
4. Kapsalis V, Karamani D: On the effect of roof added PVs on building's energy demand. Energy Build 108, 195–204(2015).
5. Al-Sabounchi A, Yalyali S, Al-Thani H: Design and performance evaluation of a PV grid-connected system in hot weather conditions. Renew Energy 53, 71-8(2013).
6. Tripanagnostopoulos Y, Nousia T, Souliotis M, Yianoulis P: Hybrid photovoltaic/thermal solar systems. Sol Energy 72, 217-234(2005).
7. Khanjari Y, Pourfayaz F, Kasaeian A: Numerical investigation on using of nanofluid in a water-cooling photovoltaic thermal system. Energy Convers Manag 122, 263-278(2016).
8. Arıcı M, Bilgin F, Nižetić S, et al.: Phase change material based cooling of photovoltaic panel: A simplified numerical model for the optimization of the phase change material layer and general economic evaluation. Journal of Cleaner Production 189, 738-745(2018).
9. Feng G, Liu S, Huang K, Pan Y, Niu R: Simulation for a new type of PV fresh air and domestic hot water system. Procedia Eng 121, 1428-34(2015).
10. Yadav A, Chandel S: Tilt angle optimization to maximize incident solar radiation: A review. Renewable and Sustainable Energy Reviews 23, 503-513(2013).
11. Zang H, Guo M, Wei Z, et al.: Determination of the optimal tilt angle of solar collectors for different climates of China. Sustainability 8(7), 654(2016).
12. Zheng J, Yin Y, Li B: A new scheme for climate regionalization in China. Acta Geographica Sinica 65(1), 3-12(2010).
13. Ong K: Thermal performance of solar air heaters: mathematical model and solution procedure. Solar energy 55(2), 93-109(1995).
14. Baljit S, Chan H, Audwinto V, Hamid S, et al.: Mathematical modelling of a dual-fluid concentrating photovoltaic-thermal (PV-T) solar collector. Renewable Energy 114, 1258-1271(2017).
15. Swinbank W: Long-wave radiation from clear skies. Quarterly Journal of the Royal Meteorological Society 89(381), 339-348(1963).
16. Duffie J, Beckman W, Blair N: Solar engineering of thermal processes, photovoltaics and wind. John Wiley & Sons, Hoboken(2020).
17. Avila K, Moxey D, De Lozar A, et al.: The onset of turbulence in pipe flow. Science 333(6039), 192-196(2011).
18. Dusenbery D: Living at micro scale: the unexpected physics of being small. Harvard University Press, Cambridge(2009).
19. Elger D, et al.: Engineering fluid mechanics. John Wiley & Sons, Hoboken(2020).
20. Bergman T, Incropera F, et al.: Fundamentals of heat and mass transfer. John Wiley & Sons, Hoboken(2011).
21. Zondag H, De Vries D, Van Helden W, et al.: The yield of different combined PV-thermal collector designs. Solar energy 74(3), 253-269(2003).

22. Nakamura H, Igarashi T: Variation of Nusselt number with flow regimes behind a circular cylinder for Reynolds numbers from 70 to 30 000. International journal of heat and mass transfer 47(23), 5169-5173(2004).
23. Yu L, et al.: Effects of aerosols and water vapour on spatial-temporal variations of the clear-sky surface solar radiation in China. Atmospheric Research 248, 105162(2021).
24. State Administration for Market Regulation, Standardization Administration of the People's Republic of China: Standards for drinking water quality, Standards Press of China, Beijing(2022).
25. Xu P.: Energy supply performance of air-, water-, and dual-cooled PV/T systems in different climatic zones of China, https://doi.org/10.21203/rs.3.rs-3190539/v1, last accessed 2023/8/22.